

# Programmable Microfluidic Synthesis of Over One Thousand Uniquely Identifiable Spectral Codes

Huy Q. Nguyen, Brian C. Baxter, Kara Brower, Camilo A. Diaz-Botia, Joseph L. DeRisi, Polly M. Fordyce,\* and Kurt S. Thorn\*

With the rise of genomic and proteomic data, high content multiplexed bioassays, which allow multiple analytes of interest to be probed and tracked in a single experiment, have become widely used for both basic research and clinical diagnosis.<sup>[1–16]</sup> While this area has traditionally been dominated by spatial microarrays, bead-based assays offer several key advantages, including rapid mixing for near fluid-phase kinetics, easier handling and manipulation, and smaller required sample volumes.<sup>[15–17]</sup> Encoded particles are attractive for biological multiplexing because they can serve as a solid-phase support for a given biological probe, thus linking the particle code to the identity of the probe and its associated analyte. Furthermore, encoded particles provide the ability to selectively cleave off probes to assess their quality or identify probe-bound material after assay completion. However, while spatial arrays of hundreds of thousands of probes have been demonstrated,<sup>[18,19]</sup> assays using encoded particles have been significantly more limited due to technical difficulties in producing more than a few hundred unique codes.

Current particle encoding strategies include spatial barcodes<sup>[7,20–26]</sup> and luminescence spectral encoding, where the spectrum of light emitted by each particle varies. Although some spatial barcoding schemes have achieved large numbers of codes, bead shape and orientation requirements during code readout have precluded widespread adoption of these schemes, especially for bioassays.<sup>[5,21,27]</sup> Spectral codes isotropically

embedded in spherical beads can be read in any orientation, making them ideal for benchtop assays. However, the available number of codes in spectrally encoded libraries has typically been relatively small. Bead-based technologies that rely on fluorescent dyes for spectral encoding (e.g., Luminex xMAP) have been reported to achieve 100–500 codes,<sup>[28–30]</sup> but these numbers approach the limit of what is theoretically possible due to spectral overlap between species. Technologies employing quantum dots (QDs) have also reached a published limit of  $\approx 100$  codes due to energy transfer between QDs when incorporated into beads.<sup>[24,31–37]</sup> Additional technical difficulties associated with using fluorophores and QDs for spectral encoding include spectral interference between the luminescent species used for encoding and for biological assay detection, the need for multiple costly excitation sources, photobleaching of the encoding species, and incompatibility with chemical reagents required for on-bead solid-phase synthesis of probe libraries.<sup>[38,39]</sup>

Lanthanide nanophosphors (LNs) offer several advantages over organic fluorophores or QDs for spectral encoding. LNs possess large Stokes shifts, resist photobleaching, and emit visible light in narrow spectral bands, making species easily distinguishable from one another.<sup>[40–44]</sup> LNs are chemically inert and relatively insensitive to environmental changes, making them compatible with common chemical conditions for bead functionalization.<sup>[40,45]</sup> Additionally, all LNs are excited at a single UV wavelength, reducing instrumentation costs and preserving the ability to use the full range of conventional fluorescent dyes for multiplexed analyte detection in downstream assays.<sup>[46]</sup> As a result, several groups have employed lanthanide-based encoding to create spatially invariant code sets up to tens of codes.<sup>[12,25,47–53]</sup> In our groups, we previously synthesized and discriminated beads containing 24 unique spectral codes created via the ratiometric incorporation of Eu-, Sm-, and Dy-doped YVO<sub>4</sub> nanophosphors within each bead.<sup>[54]</sup>

Here, we demonstrate the ability to produce and distinguish LN-doped microspheres for a code set of 1 023 distinct codes with 99.8% of beads assigned to a spectral code at 99.99% confidence with high reproducibility, representing, to our knowledge, the largest code set achieved by pure spectral encoding ever demonstrated and a 50-fold improvement from our previous work.<sup>[54]</sup> To achieve this code space, we synthesized and incorporated five brightly luminescent LN species and developed a next-generation microfluidic device for controlled, high throughput automated bead synthesis. We apply a novel computational framework to identify the embedded codes and quantitatively assess the microsphere code assignment accuracy. We anticipate that these 1000-plex encoded microspheres,

H. Q. Nguyen, B. C. Baxter, C. A. Diaz-Botia,  
J. L. DeRisi, K. S. Thorn  
Department of Biochemistry and Biophysics  
University of San Francisco  
San Francisco, CA 94158-2517, USA  
E-mail: kurt.thorn@ucsf.edu

K. Brower, P. M. Fordyce  
Department of Bioengineering  
Stanford University  
Stanford, CA 94305, USA  
E-mail: pfordyce@stanford.edu

J. L. DeRisi  
Howard Hughes Medical Institute  
Chevy Chase, MD 20815, USA

P. M. Fordyce  
Department of Genetics  
Stanford University  
Stanford, CA 94305, USA  
P. M. Fordyce  
ChEM-H  
Stanford University  
Stanford, CA 94305, USA



DOI: 10.1002/adom.201600548

which we term MRBLEs (Microspheres with Ratiometric Barcode Lanthanide Encoding), will have broad utility for high content biological assays, from genomic and proteomic biological library testing to clinical diagnosis and assessment.

MRBLEs are generated by the microfluidic production and photopolymerization of polymer droplets containing precise ratios of embedded LN species into solid polymer beads. A ratiometric encoding scheme improves code quality by enabling correction for small variations in excitation intensity and light collection efficiency across the field of view and between images. This scheme can yield a large number of unique spectral codes with a theoretical maximum limit of  $I^C$ , where  $I$  represents the number of distinct intensity levels that can be distinguished, and  $C$  represents the number of encoding species. To maximize  $I$ , we increased the brightness of individual  $\text{YVO}_4\text{:Eu}$ ,  $\text{YVO}_4\text{:Sm}$ , and  $\text{YVO}_4\text{:Dy}$  LNs  $\approx 3$ –14-fold from our previous work by removal of a bismuth codopant previously added to redshift the emission spectra (Figure S1A, Supporting Information).<sup>[54]</sup> We then increased  $C$  by synthesizing additional LN species ( $\text{YVO}_4\text{:Ho}$ ,  $\text{YVO}_4\text{:Er}$ ,  $\text{YVO}_4\text{:Tm}$ , and  $\text{LaPO}_4\text{:CeTb}$ ).<sup>[55,56]</sup> Of these,  $\text{YVO}_4\text{:Tm}$  and  $\text{LaPO}_4\text{:CeTb}$  yielded homogeneous aqueous suspensions that are brightly luminescent when excited with deep UV light (Figure 1A; Figure S1, Supporting Information), and are spectrally well-resolved from other emitting species (Figure 1B; Figure S1, Supporting Information).

We then developed a next-generation microfluidic bead synthesizer capable of high-throughput production of the millions of MRBLEs required for a  $>1000$  code set. To produce MRBLEs, individual mixtures containing polymer (polyethylene glycol diacrylate), photoinitiator,<sup>[57]</sup> a single coding LN species, and a reference LN ( $\text{Eu:YVO}_4$ ) are loaded into one of eight inputs

(Figure 1C,D). Precisely controlling the pressures driving each input (and hence their relative flow rates) generates unique ratios of lanthanides, each of which comprises a distinct spectral code. Once loaded, LN/polymer solutions are mixed via passage through a grooved herringbone channel, formed into droplets at a T-junction with a perpendicular channel flowing a surfactant/mineral oil solution (2% v/v Abil EM 90 and 0.05% v/v Span 80), and irradiated with UV light to drive polymerization into monodisperse solid beads (Figure 1E). To compensate for small code-dependent differences in solution viscosity (which can affect droplet size and code resolution), beads are synthesized in a two-step process in which LN/polymer solutions are first mixed and then pushed toward droplet generation using a single water source (Figure S2, Supporting Information). The next-generation synthesizer presented here includes two mixers and two droplet generators (Figure 1C,D; Figure S2, Supporting Information), increasing throughput  $>3$ -fold for the production of 3 000 individual MRBLEs in 2.5 min.

Embedded codes within MRBLEs are read via excitation with deep UV light (292 nm) and imaged at nine wavelengths chosen to best discriminate between individual LN emission spectra (Figure 2A). The raw images are converted to intensity images for each lanthanide by linear unmixing to determine the most likely linear combination of LNs to have produced the observed spectra at each pixel (Figure 2B). Individual MRBLE codes are then reported as the ratio of intensities of each coding LN relative to the  $\text{YVO}_4\text{:Eu}$  internal standard LN (Figure 2C). A transformation matrix is applied to register the measured ratios onto the known programmed ratios, and a Gaussian mixture model (GMM) is used to fit the mean ratios and covariance matrices that describe each code cluster, and then assign each bead to

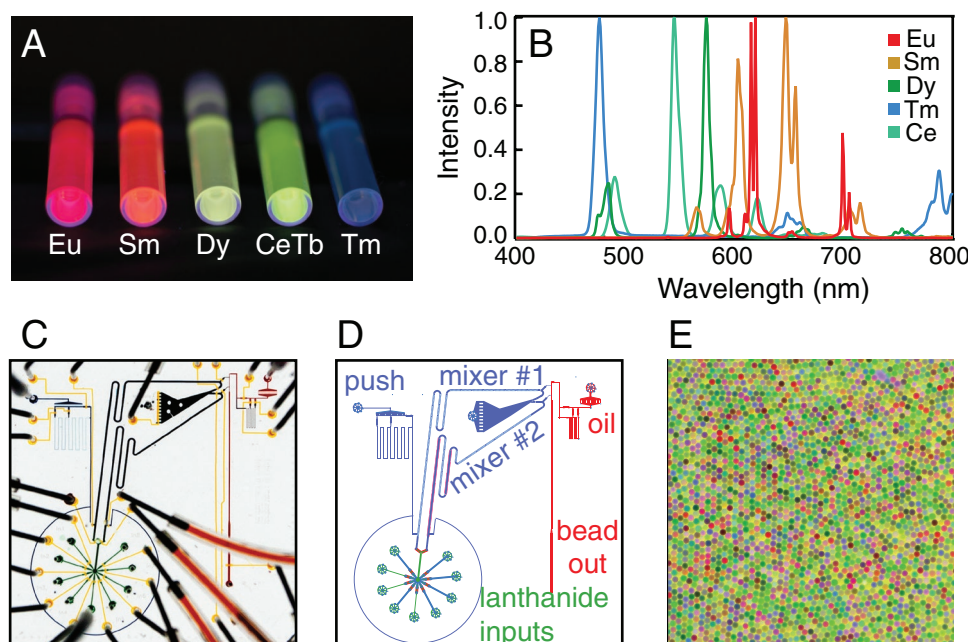


**Figure 1.** Lanthanide nanophosphor species and microfluidic devices used to generate MRBLEs. A) Photograph showing vials of  $\text{YVO}_4\text{:Eu}$ ,  $\text{YVO}_4\text{:Sm}$ ,  $\text{YVO}_4\text{:Dy}$ ,  $\text{LaPO}_4\text{:CeTb}$ , and  $\text{YVO}_4\text{:Tm}$  excited by 305 nm light from a handheld UV lamp. B) Normalized emission spectra for  $\text{YVO}_4\text{:Eu}$ ,  $\text{YVO}_4\text{:Sm}$ ,  $\text{YVO}_4\text{:Dy}$ ,  $\text{LaPO}_4\text{:CeTb}$ , and  $\text{YVO}_4\text{:Tm}$  LNs. All LNs were excited at 285 nm except for  $\text{LaPO}_4\text{:CeTb}$ , which was excited at 275 nm. C) Photograph of microfluidic bead synthesizer device used for MRBLE production. D) Cartoon schematic showing bead synthesizer device modules. E) False color image showing monodisperse microspheres from a 551 MRBLE code set.

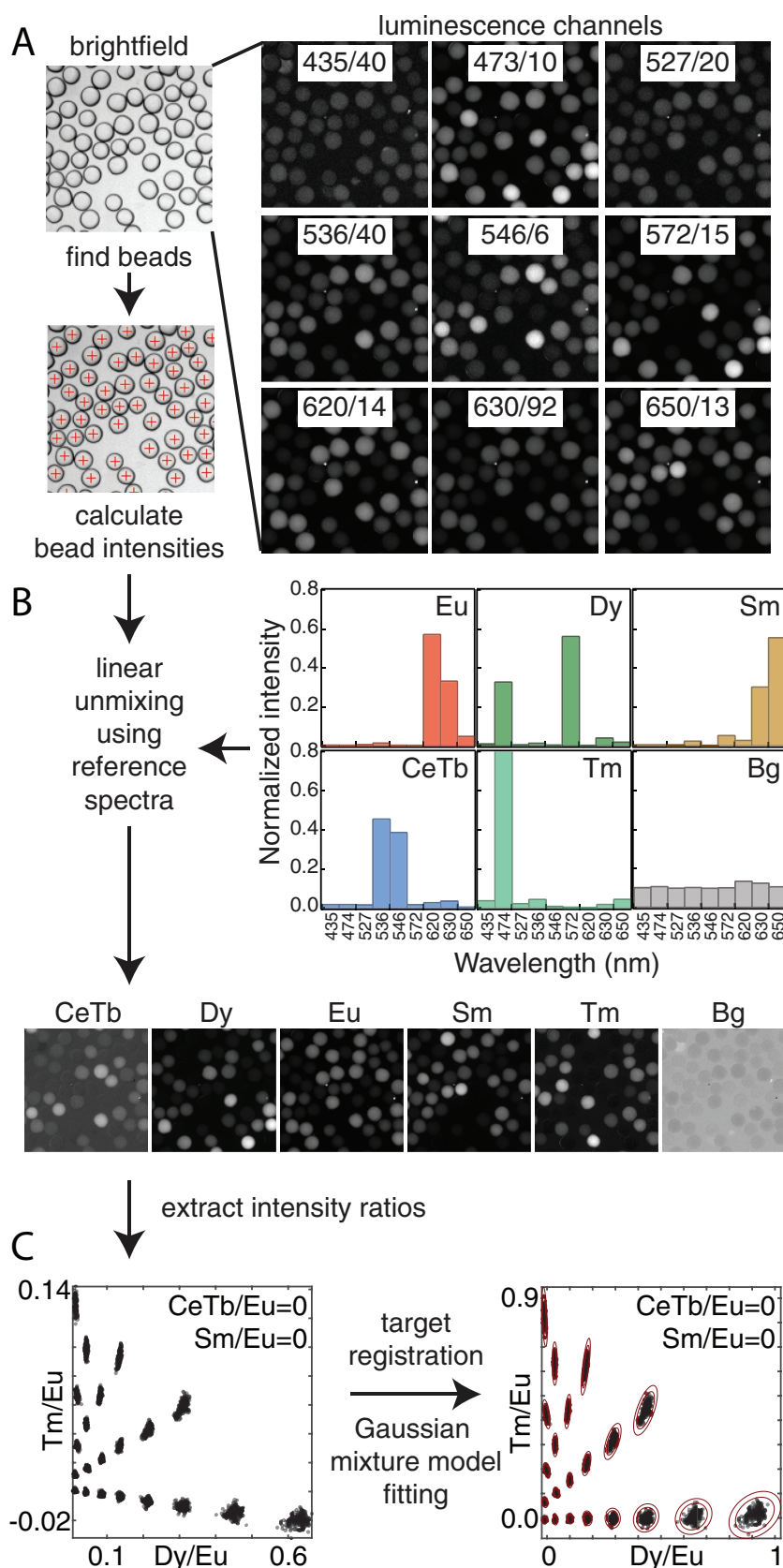


**Figure 2.** Image analysis workflow. A) Brightfield and luminescence images of MRBLES are recorded with the indicated filters; beads are identified from the brightfield image using the

its most likely code cluster (Figure 2C). Our analysis pipeline and optical instrumentation are discussed extensively in the Supporting Information.

Expanding a spectral encoding system to large numbers of codes requires careful determination of a theoretical code spacing that maximizes the number of distinct code clusters that can be resolved accurately. This optimal code spacing, in turn, depends on an accurate model of the standard deviation (SD) associated with each code cluster. In previous work using two LNs (Dy and Sm), we found that the SD of each cluster in each channel depended linearly upon only the LN level in that channel.<sup>[54]</sup> To explore whether this independence held for a larger set of lanthanide nanophosphors (Dy, Sm, Tm, and CeTb), we generated and imaged a sparse 106-code MRBLE set containing two levels of CeTb, six levels each of Dy and Sm, and five levels of Tm. Although embedded codes are identified by fitting a GMM to all dimensions simultaneously, we visualize all clusters within this 4D data set by first classifying each MRBLE by CeTb/Eu and Sm/Eu ratios (shown as columns and ratios, respectively), and then plotting their Tm/Eu ratios versus Dy/Eu ratios (Figure S3, Supporting Information). These data (from 3 185 MRBLES) demonstrate that each code forms a tight, well-separated cluster. For all LN ratios except Tm/Eu, the SD for each cluster, extracted from the GMM covariance matrix, is well fit by a linear model depending only on the mean ratio of that LN (Figure S4, Table S1, Supporting Information); for Tm/Eu, the SD for each cluster depends on both Tm/Eu and Dy/Eu ratios, likely due to overlapping emission peaks at  $\approx 470$  nm (Figure 1B; Figure S1D, Supporting Information). These empirically derived SD models allow prediction of intensity level spacings that separate code clusters by at least  $n$  SD (where  $n$  is specified by the user) to attain the maximum number of code clusters within a 4D space.

circular Hough transformation. B) Measured luminescence images are transformed into LN intensity images by linear unmixing using spectra acquired from reference MRBLES containing a single LN species. For each bead, the median intensity and median intensity ratio are recorded. C) A transformation matrix registers measured ratios to programmed ratios and a Gaussian mixture model is used to assign individual beads to a particular code. Red ellipses are the three and four standard deviation contours derived from the Gaussian mixture model covariance matrix.

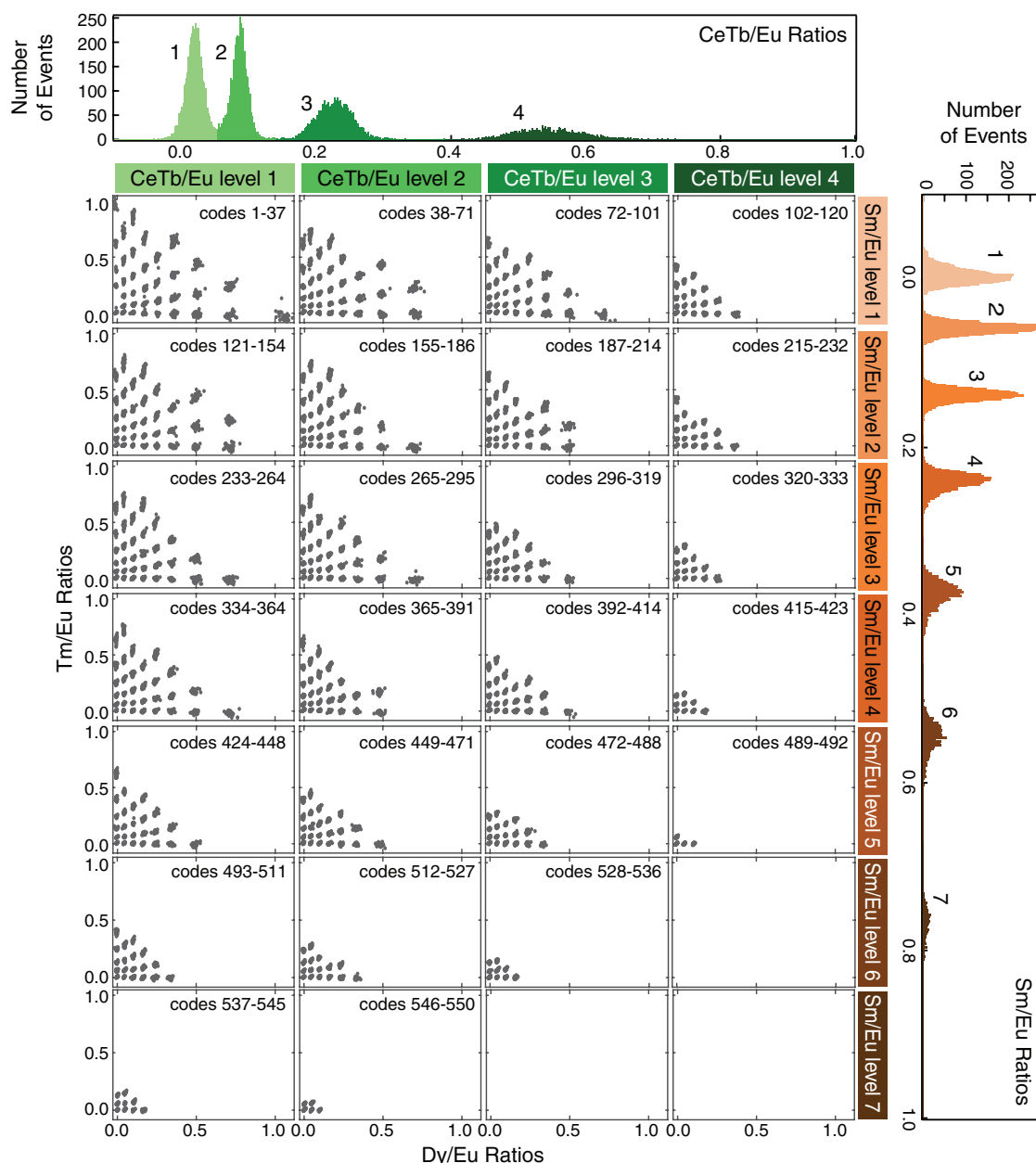


**Figure 3.** Measured intensity ratios in four dimensions for 20 801 MRBLEs from a 550 code set. MRBLEs are first separated by CeTb/Eu ratio (four columns, with each column corresponding to a single peak within the histogram of all CeTb/Eu intensities shown at top) and Sm/Eu ratio (seven rows, with each row corresponding to a single peak within the histogram of all Sm/Eu intensities shown at right). For each unique combination of CeTb/Eu and Sm/Eu ratios, a panel displays Tm/Eu ratios plotted versus Dy/Eu ratios to show individual clusters.

Using this framework, we iteratively synthesized increasingly larger code sets (Table S2, Supporting Information). We used the initial 106-code data to generate a set of 285 MRBLE codes separable by eight standard deviations (Figure S5, Supporting Information), used this 285-code data to predict a set of 341 codes separable by seven standard deviations (Figure S6, Supporting Information), and used this 341 code data to predict a set of 551 codes separable by 5.7 standard deviations. **Figure 3** shows the 4D data from 20 801 MRBLEs from this 551-code MRBLE set comprised of 4 CeTb levels, 9 Dy levels, 7 Sm levels, and 7 Tm levels; the full set of intensity histograms for

each channel is shown in Figure S7 (Supporting Information). As with the sparser code sets, MRBLEs fall into discrete clusters that are well separated from their neighbors, although one cluster is missing due to a production error. This demonstration of 550 codes surpasses all known purely spectral encoding libraries published to date.

We hypothesized that our library size could be further increased by synthesizing several sets of MRBLEs, each containing a different Eu reference level as an additional coding parameter. To test this, we verified that different Eu levels could be easily resolved from one another (Figure S8, Supporting



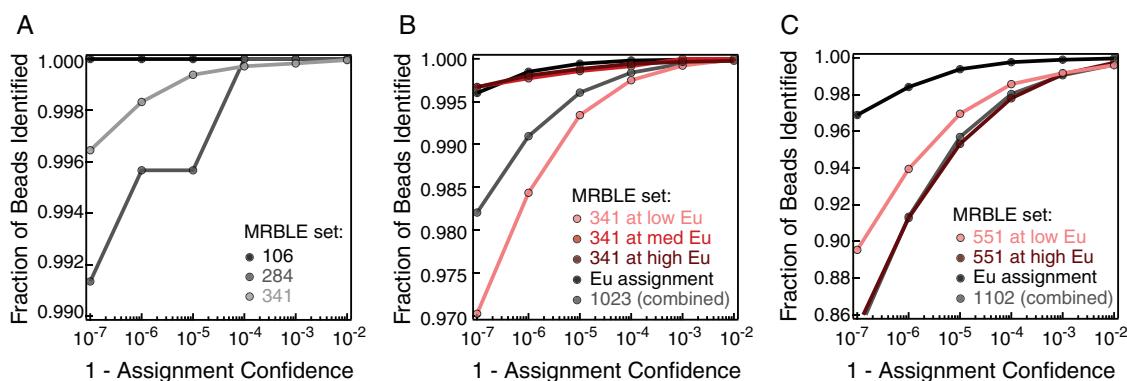


**Figure 4.** A) Confidence plots for MRBLE code assignment. B) Plot showing the fraction of MRBLEs that can be identified with a given confidence level for 50 564 MRBLEs from a 1 101 code set containing two distinct Eu levels (20 801 with 100% Eu and 29 853 with 50% Eu). C) Plot showing the fraction of MRBLEs that can be identified with a given confidence level for MRBLEs from a 1 023 code set containing three distinct Eu levels (16 419 with 25% Eu, 7 008 with 50% Eu, and 16 932 with 100% Eu).

Information) and synthesized additional code sets containing either two or three different levels of Eu. First, we synthesized an additional 551 code MRBLEs containing 40% of the standard Eu reference level and combined it with the 550 code MRBLEs above to create a composite set of 1 101 codes (Figure 3; Figure S9 and Movie S1, Supporting Information). Second, we created three 341-code MRBLE sets containing either 100%, 50%, or 25% of the standard Eu reference and combined them to create a composite set of 1 023 codes (Figures S10–S12, Supporting Information).

For small numbers of codes, code quality is often established by simply plotting histograms or clusters of intensities and visually assessing whether it seems possible to unambiguously assign a code to any given bead. To evaluate the quality of these large code sets spanning 5D space, we developed a new quantitative framework similar to a receiver operating characteristic curve. First, we assess the likelihood of a MRBLE belonging to each code using the posterior probabilities returned by the Gaussian mixture model described above. For MRBLEs with varying reference Eu levels, we multiply this posterior code probability by the probability of the Eu level assignment. For a given probability, we then globally assess code quality by determining the fraction of MRBLEs assigned to their most likely code with that probability or higher. For the 1 023 code set, 99.8% of MRBLEs can be assigned to a code with 99.99% confidence and 99.9% of MRBLEs to a code with 99.9% confidence (Figure 4B; Table S2, Supporting Information). For the 1 101 code set, 98.0% of MRBLEs can be assigned to a code with 99.99% confidence and 99.1% of MRBLEs to a code with 99.9% confidence (Figure 4C; Table S2, Supporting Information). Smaller code sets can be assigned with even higher accuracies; e.g., for a 341-code set, we can assign 99.97% of MRBLEs to a code with 99.99% confidence (Figure 4A; Table S2, Supporting Information). Taken together, these assignment rates far exceed all existing technologies to date known to us from the literature.

In conclusion, we have demonstrated the ability to synthesize MRBLEs with over 1 000 unique spectral barcodes, representing the largest code set created using purely spectral encoding to date. We further developed a quantitative metric for globally assessing code quality, which is broadly applicable to benchmarking many encoded particle technologies beyond that

presented here. In total, we have shown data for six different sets of MRBLEs ranging from 106 to 1 101 codes in size, with assignment accuracies ranging from 100% assignment to 98% assignment at 99.99% confidence.

While commercial fluorophore-based technologies are approaching their theoretical encoding limit due to spectral overlap, this lanthanide-based encoding system has significant potential for future growth to even larger code sets. First, coding capacity can be increased by incorporating upconverting LNs, which are excited with infrared light (typically at 980 nm) and emit visible light in narrow, well-defined spectral bands.<sup>[58–62]</sup> Two popularly synthesized upconverting species (NaYF<sub>4</sub>:YbEr and NaYF<sub>4</sub>:YbTm) are spectrally orthogonal to the downconverting LNs employed here as well as fluorophores commonly used for bound analyte detection, rendering them ideal for achieving  $>10^4$  distinct codes. Second, accounting for the observed covariance between LN ratios within each code would allow tighter packing of code clusters off of the orthogonal grid we currently use. Finally, we present here a rigorous code separation method to demonstrate the potential of downconverting LNs for creating extremely large code spaces. In future practical applications, it is likely that we can tolerate a lower assignment confidence that what we observe here, thereby achieving even larger numbers of codes. In summation, MRBLEs represent a promising lanthanide-based encoding technology that enables spectral encoding to reach unprecedented numbers of codes, and anticipate this system will ultimately prove useful for a broad range of microsphere-based multiplexed bioassays.

## Supporting Information

Supporting Information is available from the Wiley Online Library or from the author.

## Acknowledgements

H.Q.N. and B.C.B. contributed equally to this work. The authors thank Marshall Burke for device photography and Zev Bryant for helpful comments on the manuscript. Funding for this work was provided in part by NIH/NIGMS grant R01GM107132, the Howard Hughes Medical

Institute, a seed grant from the Stanford ChEM-H Institute, and by a W.M. Keck Foundation grant. Portions of this work were performed as a user project at the Molecular Foundry and were supported by the Office of Basic Energy Science, of the U.S. Department of Energy under Contract No. DE-AC02-05CH11231. The authors acknowledge the work of Parallel Synthesis Technologies, Inc. and Robert Haushalter within the field of optical encoding. See U.S. Patent no. 8,796,030, 8,673,107, and 8,927,892.

Received: July 11, 2016  
Revised: August 3, 2016  
Published online:

- [1] S. Birtwell, H. Morgan, *Integr. Biol.* **2009**, *1*, 345.
- [2] G. R. Broder, R. T. Ranasinghe, J. K. She, S. Banu, S. W. Birtwell, G. Cavalli, G. S. Galitonov, D. Holmes, H. F. P. Martins, K. F. MacDonald, C. Neylon, N. Zheludev, P. L. Roach, H. Morgan, *Anal. Chem.* **2008**, *80*, 1902.
- [3] K. B. Cederquist, S. L. Dean, C. D. Keating, *WIREs Nanomed. Nanobiotechnol.* **2010**, *2*, 578.
- [4] G. A. Lawrie, B. J. Battersby, M. Trau, *Adv. Funct. Mater.* **2003**, *13*, 887.
- [5] H. Lee, J. Kim, H. Kim, J. Kim, S. Kwon, *Nat. Mater.* **2010**, *9*, 745.
- [6] G. C. Le Goff, R. L. Srinivas, W. A. Hill, P. S. Doyle, *Eur. Polym. J.* **2015**, *72*, 386.
- [7] L. N. Kim, M. Kim, K. Jung, H. J. Bae, J. Jang, Y. Jung, J. Kim, S. Kwon, *Chem. Commun.* **2015**, *51*, 12130.
- [8] S. C. Chapin, D. C. Appleyard, D. C. Pregibon, P. S. Doyle, *Angew. Chem. Int. Ed.* **2011**, *50*, 2289.
- [9] D. C. Appleyard, S. C. Chapin, P. S. Doyle, *Anal. Chem.* **2011**, *83*, 193.
- [10] J. P. Nolan, F. Mandy, *Cytometry* **2006**, *69A*, 318.
- [11] C. T. Lim, Y. Zhang, *Biosens. Bioelectron.* **2007**, *22*, 1197.
- [12] F. Zhang, R. C. Haushalter, R. W. Haushalter, Y. Shi, Y. Zhang, K. Ding, D. Zhao, G. D. Stucky, *Small* **2011**, *7*, 1972.
- [13] F. Zhang, Q. Shi, Y. Zhang, Y. Shi, K. Ding, D. Zhao, G. D. Stucky, *Adv. Mater.* **2011**, *23*, 3775.
- [14] Y. Zhao, Y. Cheng, L. Shang, J. Wang, Z. Xie, Z. Gu, *Small* **2015**, *11*, 151.
- [15] K. Braeckmans, S. C. De Smedt, M. Leblans, R. Pauwels, J. Demeester, *Nat. Rev. Drug Discov.* **2002**, *1*, 447.
- [16] N. H. Finkel, X. Lou, C. Wang, L. He, *Anal. Chem.* **2004**, *76*, 352 A.
- [17] R. Wilson, A. R. Cossins, D. G. Spiller, *Angew. Chem. Int. Ed. Engl.* **2006**, *45*, 6104.
- [18] M. J. Heller, *Annu. Rev. Biomed. Eng.* **2002**, *4*, 129.
- [19] J. B. Legutki, Z.-G. Zhao, M. Greving, N. Woodbury, S. A. Johnston, P. Stafford, *Nat. Commun.* **2014**, *5*, 1.
- [20] S. R. Nicewarner-Peña, R. G. Freeman, B. D. Reiss, L. He, D. J. Peña, I. D. Walton, R. Cromer, C. D. Keating, M. J. Natan, *Science* **2001**, *294*, 137.
- [21] M. J. Dejneka, A. Streltsov, S. Pal, A. G. Frutos, C. L. Powell, K. Yost, P. K. Yuen, U. Müller, J. Lahiri, *Proc. Natl. Acad. Sci. USA* **2003**, *100*, 389.
- [22] S. Fournier Bidoz, T. L. Jennings, J. M. Klostranec, W. Fung, A. Rhee, D. Li, W. C. W. Chan, *Angew. Chem. Int. Ed.* **2008**, *47*, 5577.
- [23] X.-H. Ji, N.-G. Zhang, W. Cheng, F. Guo, W. Liu, S.-S. Guo, Z.-K. He, X.-Z. Zhao, *J. Mater. Chem.* **2011**, *21*, 13380.
- [24] Y. Zhao, H. C. Shum, H. Chen, L. L. A. Adams, Z. Gu, D. A. Weitz, *J. Am. Chem. Soc.* **2011**, *133*, 8790.
- [25] J. Lee, P. W. Bisso, R. L. Srinivas, J. J. Kim, A. J. Swiston, P. S. Doyle, *Nat. Mater.* **2014**, *13*, 524.
- [26] D. Falconnet, J. She, R. Tornay, E. Leimgruber, D. Bernasconi, L. Lagopoulos, P. Renaud, N. Demierre, P. van den Bogaard, *Anal. Chem.* **2015**, *87*, 1582.
- [27] K. Braeckmans, S. C. De Smedt, C. Roelant, M. Leblans, R. Pauwels, J. Demeester, *Nat. Mater.* **2003**, *2*, 169.
- [28] B. Houser, *Arch. Physiol. Biochem.* **2012**, *118*, 192.
- [29] Y. Zhang, R. Birru, Y. P. Di, in *Molecular Toxicology Protocols*, Humana Press, Totowa, NJ **2014**, pp. 43–57.
- [30] S. A. Dunbar, *Clin. Chim. Acta* **2006**, *363*, 71.
- [31] S. Fournier Bidoz, T. L. Jennings, J. M. Klostranec, W. Fung, A. Rhee, D. Li, W. C. W. Chan, *Angew. Chem. Int. Ed.* **2008**, *47*, 5577.
- [32] X. Gao, S. Nie, *J. Phys. Chem. B* **2003**, *107*, 11575.
- [33] S. W. Han, E. Jang, W.-G. Koh, *Sens. Actuators: B. Chem.* **2015**, *209*, 242.
- [34] X.-H. Ji, W. Cheng, F. Guo, W. Liu, S.-S. Guo, Z.-K. He, X.-Z. Zhao, *Lab Chip* **2011**, *11*, 2561.
- [35] Y. Zhao, Z. Xie, H. Gu, L. Jin, X. Zhao, B. Wang, Z. Gu, *NPG Asia Mater.* **2012**, *4*, e25.
- [36] S. Shojaei-Zadeh, J. F. Morris, A. Couzis, C. Maldarelli, *J. Colloid and Interf. Sci.* **2011**, *363*, 25.
- [37] M. Han, X. Gao, J. Z. Su, S. Nie, *Nat. Biotechnol.* **2001**, *19*, 631.
- [38] F. Wang, W. B. Tan, Y. Zhang, X. Fan, M. Wang, *Nanotechnology* **2005**, *17*, R1.
- [39] Y. Leng, K. Sun, X. Chen, W. Li, *Chem. Soc. Rev.* **2015**, *44*, 5552.
- [40] C. R. Ronda, T. Jüstel, H. Nikol, *J. Alloys Compounds* **1998**, *275–277*, 669.
- [41] H. Xu, H. Wang, Y. Meng, H. Yan, *Solid State Commun.* **2004**, *130*, 465.
- [42] W. Xu, H. Song, D. Yan, H. Zhu, Y. Wang, S. Xu, X. Bai, B. Dong, Y. Liu, *J. Mater. Chem.* **2011**, *21*, 12331.
- [43] X. Lim, *Nat. News* **2016**, *531*, 26.
- [44] S. Petoud, S. M. Cohen, J.-C. G. Bünzli, K. N. Raymond, *J. Am. Chem. Soc.* **2003**, *125*, 13324.
- [45] M. Lin, Y. Zhao, S. Q. Wang, M. Liu, Z. F. Duan, Y. M. Chen, F. Li, F. Xu, T. J. Lu, *Biotechnol. Adv.* **2012**, *30*, 1551.
- [46] J.-C. G. Bünzli, C. Piguet, *Chem. Soc. Rev.* **2005**, *34*, 1048.
- [47] H. H. Gorris, R. Ali, S. M. Saleh, O. S. Wolfbeis, *Adv. Mater.* **2011**, *23*, 1652.
- [48] P. Schuetz, F. Caruso, *Chem. Mater.* **2002**, *14*, 4509.
- [49] N. Wartenberg, O. Raccurt, D. Imbert, M. Mazzanti, E. Bourgeat-Lami, *J. Mater. Chem. C* **2013**, *1*, 2061.
- [50] R. C. Haushalter, Parallel Synthesis Technologies, Inc., US Patent 8,673,107, **2014**.
- [51] R. C. Haushalter, Parallel Synthesis Technologies, Inc., US Patent 8,796,030, **2014**.
- [52] R. W. Haushalter, R. C. Haushalter, Parallel Synthesis Technologies, Inc., US 8,927,892, **2015**.
- [53] Parallel Synthesis Technologies, [www.parallel-synthesis.com](http://www.parallel-synthesis.com) (accessed: September 2016).
- [54] R. E. Gerver, R. Gómez-Sjöberg, B. C. Baxter, K. S. Thorn, P. M. Fordyce, C. A. Diaz-Botia, B. A. Helms, J. L. DeRisi, *Lab Chip* **2012**, *12*, 4716.
- [55] V. Buisette, M. Moreau, T. Gacoin, J.-P. Boilot, J.-Y. Chane-Ching, T. Le Mercier, *Chem. Mater.* **2004**, *16*, 3767.
- [56] V. Buisette, D. Giaume, T. Gacoin, J.-P. Boilot, *J. Mater. Chem.* **2006**, *16*, 529.
- [57] B. D. Fairbanks, M. P. Schwartz, C. N. Bowman, K. S. Anseth, *Biomaterials* **2009**, *30*, 6702.
- [58] W. Feng, C. Han, F. Li, *Adv. Mater.* **2013**, *25*, 5287.
- [59] S. X. J. Z. J. Q. Jiajia Zhou, *Nanoscale* **2015**, *7*, 15026.
- [60] F. Zhang, in *Photon Upconversion Nanomaterials*, Springer Berlin Heidelberg, Berlin/Heidelberg, Germany **2014**, pp. 233–253.
- [61] M. Lin, Y. Zhao, S. Wang, M. Liu, Z. F. Duan, Y. Chen, F. Li, F. Xu, T. Lu, *Biotechnol. Adv.* **2012**, *30*, 1551.
- [62] K. Huang, N. M. Idris, Y. Zhang, *Small* **2015**, *12*, 836.